Molecular Therapy
Nucleic Acids
Original Article

Hypoxic ucMSC-secreted exosomal miR-125b promotes endothelial cell survival and migration during wound healing by targeting TP53INP1

Xiao-Fei Zhang,[1] Ting Wang,[2] Zi-Xuan Wang,[3] Kun-Peng Huang,[3] Yun-Wei Zhang,[4] Guo-Liang Wang,[5] Hong-Ji Zhang,[3] Zi-Han Chen,[2] Chang-Yan Wang,[2] Jin-Xiang Zhang,[3] and Hui Wang[2]

[1]Center for Translational Medicine, Union Hospital, Tongji Medical College, Huazhong University of Science and Technology, Wuhan 430022, China; [2]Department of Medical Genetics, Basic school of Tongji Medical College, Huazhong University of Science and Technology, 13 Hangkong Road, Wuhan 430030, China; [3]Department of Emergency Surgery, Union Hospital, Tongji Medical College, Huazhong University of Science and Technology, Wuhan 430022, China; [4]Department of Emergency, Union Hospital, Tongji Medical College, Huazhong University of Science and Technology, Wuhan 430022, China; [5]Department of Hepatobiliary Surgery, Union Hospital, Tongji Medical College, Huazhong University of Science and Technology, Wuhan 430022, China

A hypoxic microenvironment is a common feature of skin wounds. Our previous study demonstrated that three-dimensional coculture of umbilical cord-derived mesenchymal stem cells (ucMSCs) and endothelial cells facilitates cell communication and host integration in skin tissue engineering. Here, we aimed to identify the mechanism by which ucMSCs affect endothelial cells under hypoxic conditions after skin injury. We demonstrate that hypoxia enhances the exosome-mediated paracrine function of ucMSCs, which increases endothelial cell proliferation and migration. In a mouse full-thickness skin injury model, ucMSC-derived exosomes can be taken up by endothelial cells and accelerate wound healing. Hypoxic exosomes lead to a better outcome than normoxic exosomes by promoting proliferation and inhibiting apoptosis. Mechanistically, microRNA-125b (miR-125b) transcription is induced by hypoxia in ucMSCs. After being packaged into hypoxic exosomes and transported to endothelial cells, miR-125b targets and suppresses the expression of tumor protein p53 inducible nuclear protein 1 (TP53INP1) and alleviates hypoxia-induced cell apoptosis. Inhibition of miR-125b-TP53INP1 interaction attenuates the protective effect of hypoxic exosomes. Moreover, artificial agomiR-125b can accelerate wound healing *in vivo*. Our findings reveal communication between ucMSCs and endothelial cells via exosomal miR-125b/TP53INP1 signaling in the hypoxic microenvironment and present hypoxic exosomes as a promising therapeutic strategy to enhance cutaneous repair.

INTRODUCTION

Skin, an effective barrier that prevents body dehydration and external microorganism penetration, is extremely vulnerable to different types of lesions, such as burns, ulcers, and wounds. Stem cell-based skin tissue engineering has shown great promise for wound healing.[1–3] Mesenchymal stem cells (MSCs) exist in many adult tissues, such as the bone marrow, adipose tissue, and umbilical cords (UCs).[4] Among the types of MSCs, umbilical cord MSCs (ucMSCs) are advantageous because their collection causes no risk or discomfort to the donor, and they have a highly similar gene expression pattern to that of skin fibroblasts;[5,6] thus, ucMSCs have a substantial potential in skin wound repair or tissue engineering. However, the clinical application of ucMSCs still faces several problems, such as the low cell viability of transplanted cells and the risk of immune responses in recipients.[7]

Exosomes (Exos) derived from MSCs exhibit similar functions to MSCs, but have their own set of advantages, such as their anti-inflammatory, anti-apoptotic, and angiogenesis-promoting effects.[8,9] Exosomes are lipid bilayer vesicles containing mRNAs, microRNAs (miRs), lipids, and proteins.[10,11] By delivering various RNAs and proteins to neighboring or distant cells, exosomes play an important role in cell-cell communication and disease progression.[10,11] The administration of exosomes is considered an attractive cell-free approach to tissue repair and organ regeneration.[12–14] However, the composition of exosomes varies widely according to the parent cells from which they are derived and is profoundly affected by physiological and pathological conditions, such as mechanical or metabolic stresses, hypoxia, or abnormal pH.[15–17] During skin injury, a condition of hypoxia arises. The exosomes secreted by ucMSCs under hypoxic conditions are significantly different from those secreted under normoxic conditions, including the enrichment of specific types of miR-21 and miR-23a.[18,19] However, whether hypoxic ucMSC-derived exosomes have a special function in skin wound healing remains to be further elucidated.

Received 29 January 2021; accepted 17 July 2021;
https://doi.org/10.1016/j.omtn.2021.07.014.

Correspondence: Hui Wang, Department of Medical Genetics, Basic school of Tongji Medical College, Huazhong University of Science and Technology, 13 Hangkong Road, Wuhan 430030, China.
E-mail: wanghuipitt@hust.edu.cn

Endothelial cells play a vital role in skin repair. The locally hypoxic environment in wounds enhances the proliferation and migration of endothelial cells to induce revascularization.[20,21] We previously co-cultured ucMSCs and endothelial cells in a three-dimensional gelatin methacryloyl hydrogel to construct engineered skin analogs. We found that three-dimensional coculture of the two types of cells markedly enhanced the gene expression levels of *CHD1*, *FGF2*, and *VEGFA in vitro* and promoted host integration *in vivo* when compared with culture of ucMSCs or endothelial cells alone; these results suggested that cell-cell communication might be beneficial to angiogenesis and tissue regeneration.[22] Given that hydrogels also create a hypoxic environment for cells, we postulated that the communication between ucMSCs and endothelial cells under hypoxic conditions might be a favorable factor for skin repair.

Here, we found that hypoxia enhanced the paracrine effect of ucMSCs on endothelial cell proliferation and migration *in vitro*, and the impact of ucMSCs on endothelial cells was mediated by exosomes. Mechanistically, miR-125b enriched in hypoxic exosomes was a key molecule that promoted the survival and migration of endothelial cells. Our study further reveals that exosomal-miR-125b/TP53INP1 signaling is crucial for the communication of ucMSCs and endothelial cells, which provides a therapeutic target for exosome-based cell-free skin tissue engineering.

RESULTS

ucMSC-derived exosomes mediate the paracrine effect of ucMSCs on the cell proliferation and migration of endothelial cells under hypoxic conditions

To investigate the role of hypoxia in the interaction of ucMSCs and endothelial cells, we treated human umbilical vein endothelial cells (HUVECs) with the supernatants from ucMSCs cultured under normoxic or hypoxic conditions. The results from the Cell Counting Kit-8 (CCK-8) assay showed that both the normoxic and hypoxic supernatants of ucMSCs increased the viability of HUVECs, and the hypoxic supernatants resulted in higher cell viability than the normoxic supernatants (Figure 1A). The migration of endothelial cells plays an important role in tissue repair. To study the effect of the hypoxic supernatants of ucMSCs on HUVEC migration, we performed wound healing and Transwell migration assays. The wound-healing assay demonstrated that the hypoxic supernatants of ucMSCs increased cell migration, as indicated by the significantly smaller wound area in the hypoxic group than in the normoxic group at 16 h (Figure 1B). Then, an indirect coculture model using a Transwell system was established (Figure 1C). The HUVECs exposed to the hypoxic supernatants of ucMSCs displayed the greatest migratory ability among the three groups of cells (Figure 1C). These data indicated that hypoxia promoted the paracrine effect of ucMSCs on the proliferation and migration of endothelial cells.

Exosomes, as major paracrine components of mesenchymal stem cells, mediate intercellular communication in various physiological or pathological processes.[23–25] To further explore the role of exosomes in the paracrine function of ucMSCs, we pretreated ucMSCs with GW4869 (10 μM, an inhibitor of exosome biogenesis and release) for 48 h. The culture media were replaced by fresh complete media, and the cells were exposed to hypoxic conditions for 12 h. Then, the supernatants were harvested to treat HUVECs. The CCK-8 assay showed that GW4869 pretreatment significantly blocked the promoting effect of ucMSCs on the viabilities of HUVECs (Figure 1D), demonstrating that exosomes are an essential mediator of ucMSC functions. Then, ucMSCs were cultured for 72 h under normoxic and hypoxic conditions, and normoxic and hypoxic exosomes were isolated from the culture media by ultracentrifugation. The particle size and zeta potential of the normoxic and hypoxic exosomes were assessed by a particle detector. In good agreement with the range of standard values of exosomes, the average diameters of the two types of exosomes were within 104.2~118.5 nm (Figure 1E), and the average zeta potential value ranged from −3.9~−6.9 mV (Figure 1F). Under transmission electron microscopy, the two types of exosomes displayed representative cup-shaped morphology (Figure 1G), which was consistent with previous reports.[25,26] Known exosomal markers, including CD9, CD63, CD81, and HSP70, were also expressed in both types of exosomes (Figure 1H). Then, exosomes labeled with 3,3′-dioctadecyloxacarbocyanine perchlorate (DIOC18(3), a green fluorescent lipophilic tracer) were used to treat HUVECs. The images showed that HUVECs indeed took up the exosomes, which were mainly distributed in the perinuclear region of HUVECs (Figure 1I). Then, exosomes were added to the culture media of HUVECs to determine their effect on the function of endothelial cells. As Figures 1J and 1K show, hypoxic exosomes induced higher endothelial cell viabilities and migratory activities than normoxic exosomes. These data indicated that exosomes derived from ucMSCs mediated the paracrine effect of ucMSCs on HUVECs, and the hypoxic microenvironment in local wounds might create a favorable context for the function of ucMSCs.

Hypoxic exosomes lead to a better outcome of regenerated skin by enhancing cell proliferation and inhibiting cell apoptosis compared to normoxic exosomes

A mouse full-thickness cutaneous injury model was established to verify the effect of normoxic or hypoxic exosomes on wound healing. The wounds were photographed, and wound healing curves were generated. As shown in Figure 2A, the wound areas in both normoxic and hypoxic exosome-treated groups were smaller than those in the PBS-treated group at day 3 and day 8, and the wounds of the three groups almost healed at day 12. Statistical analysis showed the faster healing rates of the normoxic and hypoxic exosome-treated groups than of the PBS group, while the healing rate of the hypoxic exosome-treated group was very close to that of the normoxic exosome-treated group (Figure 2B). With an *in vivo* tracking assay, we observed a remarkable colocalization of exosomes (DIOC18(3), green) and endothelial cells (von Willebrand factor, red) at the areas adjacent to the injury sites, which confirmed the uptake of exosomes by endothelial cells (Figure 2C). Hematoxylin and eosin (H&E) staining also showed that there were no statistically significant differences in the thickness of the epidermis among normoxic exosome-, hypoxic exosome-, and PBS-treated groups; however, the epidermis in both

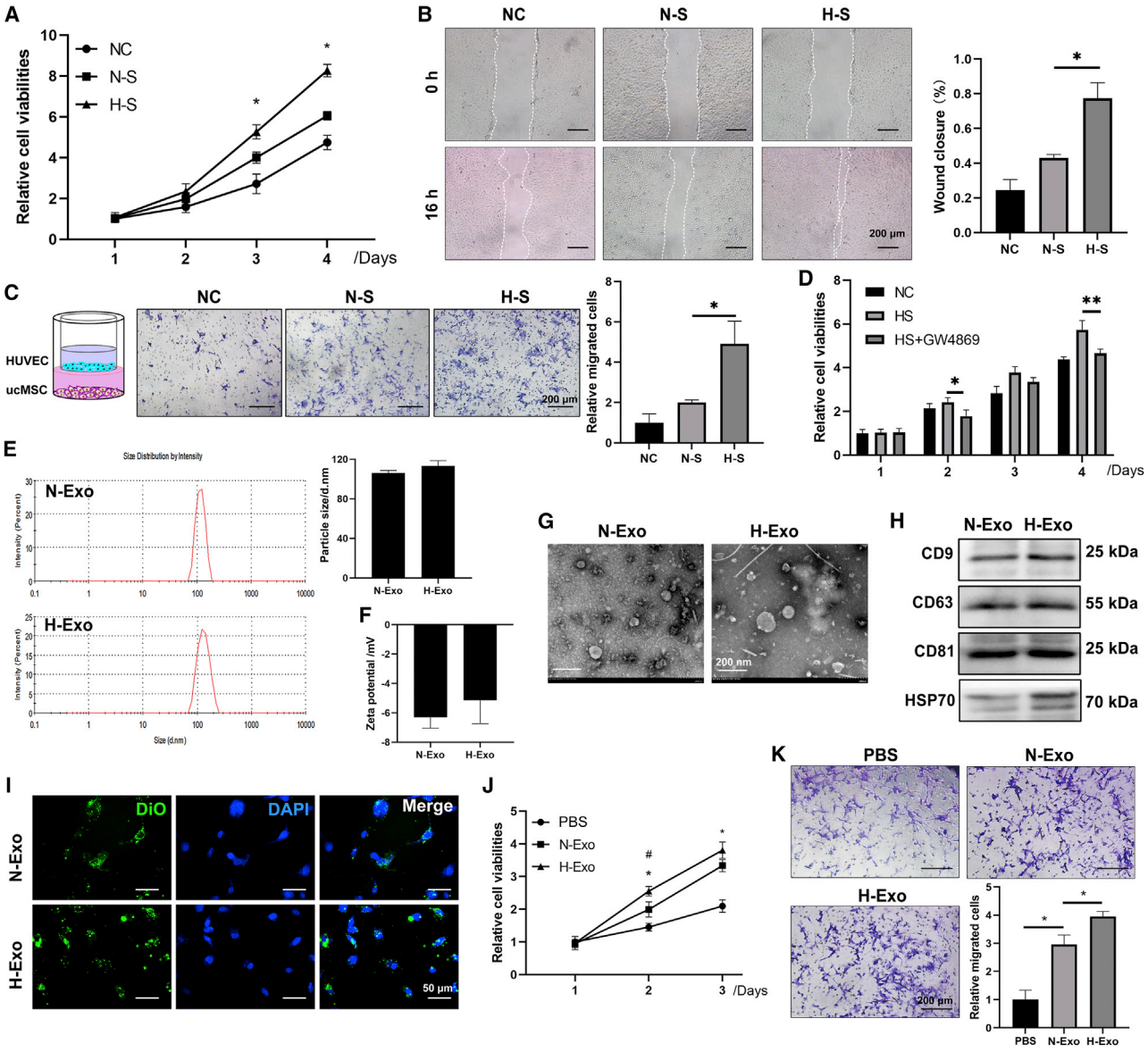

Figure 1. ucMSC-derived exosomes induce proliferation and migration of endothelial cells under hypoxic conditions

HUVECs were treated with NC (complete media without serum), N-S (the supernatants of ucMSCs cultured under normoxic conditions without serum), and H-S (the supernatants of ucMSCs cultured under hypoxic conditions without serum) for the indicated times. (A) CCK-8 analysis of cell proliferation of HUVECs. *$p < 0.05$, N-S group versus H-S group. (B and C) Wound-healing assay (B) and Transwell assay (C) of the migratory activities of HUVECs. Scale bar, 200 μm; *$p < 0.05$. (D) ucMSCs were pretreated with GW4869 (10 μM) for 48 h. The culture media were replaced with fresh complete media, and the cells were exposed to hypoxia for 12 h. Then, the supernatants were used to treat HUVECs. CCK-8 analysis of cell proliferation of HUVECs. *$p < 0.05$, **$p < 0.01$. (E and F) Particle size distribution (E) and zeta potential (F) of normoxic exosomes (N-Exos) or hypoxic exosomes (H-Exos). (G) Morphology of normoxic and hypoxic exosomes photographed by transmission electron microscopy. Scale bar, 200 nm. (H) Western blotting of the expression of the surface markers CD9, CD63, CD81, and HSP70 in equal amounts of normoxic and hypoxic exosomes. (I) The internalization of DIOC18(3)-labeled exosomes by HUVECs. Scale bar, 50 μm. (J) CCK-8 assay of HUVECs treated with normoxic or hypoxic exosomes. *$p < 0.05$ versus PBS treated group, #$p < 0.05$ versus normoxic exosome group. (K) Transwell migration assay of HUVECs treated with normoxic or hypoxic exosomes. Scale bar, 200 μm; *$p < 0.05$. The data are presented as the mean ± SD.

the normoxic (26.4 ± 2.9 μm) and hypoxic (27.3 ± 9.8 μm) exosome-treated groups was slightly thinner than that in the PBS group (30.4 ± 4.5 μm) (Figure 2D). Ki67 and TUNEL staining were performed to evaluate cell proliferation and apoptosis (Figure 2D). The exosome injection groups had significantly more Ki67-positive cells and fewer TUNEL-positive cells than the PBS control group. Interestingly, we

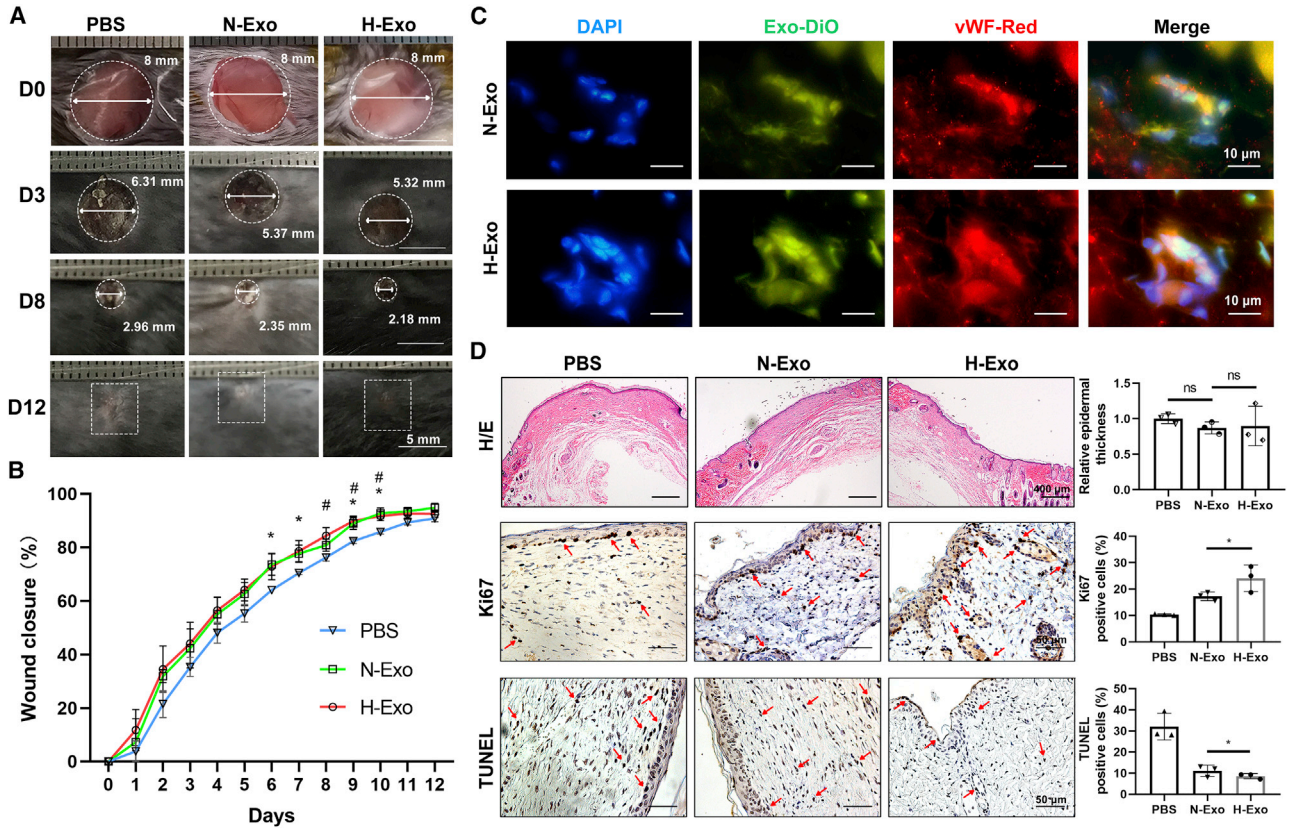

Figure 2. Hypoxic exosomes improve the outcome of wound healing in a mouse full-thickness skin injury model

(A) Gross view of wound areas of mice injected with normoxic or hypoxic exosomes. Scale bar, 5 mm. Line segments with arrows represent the diameters of wound areas. The wound areas at D0, D3, and D8 are outlined with a circular dotted box, and with a square dotted box at D12 due to the difficulty in defining the border. (B) Quantification of wound closure rates. n = 5. *p < 0.05, normoxic exosome-treated group versus PBS-treated group; #p < 0.05, hypoxic exosome-treated group versus PBS-treated group. (C) *In vivo* uptake of DIOC18(3)-labeled exosomes (GFP) by HUVECs (von Willebrand factor, red). Scale bar, 10 μm. (D) Representative images of H&E staining, Ki67 staining, and TUNEL staining, and quantitative analysis of the thickness of newly formed epidermis, the number of Ki67-positive cells, and the number of TUNEL-positive cells at the end point of wound repair (day 12). Scale bar, 400 μm in H&E staining and 50 μm in Ki67 and TUNEL staining. ns, no significance. *p < 0.05. The data are presented as the mean ± SD.

observed a significantly increased number of Ki67-positive cells and a decreased number of TUNEL-positive cells in the hypoxic exosome-treated group compared to the normoxic exosome-treated group (Figure 2D), suggesting a better outcome of hypoxic exosome treatment.

ucMSC-derived exosomal miR-125b, transcriptionally induced by hypoxia, modulates the behaviors of endothelial cells

Exosomes always carry and deliver mRNAs, microRNAs, and proteins to target cells, and the levels of exosome contents are strongly correlated with their levels in the cells of origin.[27,28] Hypoxic conditions have been implicated in modulating the expression profile of microRNAs in different types of cells as well as in the exosomes derived from these cells.[29–31] A previous study investigated the exosomal microRNA expression profile in ucMSCs and screened several abundant microRNAs, including miR-21-5p, miR-125b-5p, miR-23a-3p, let-7f-5p, let-7a-5p, and miR-145-5p.[18] We speculated that the abundance of microRNAs in exosomes was important for their functions, so we confirmed the expression of these microRNAs and analyzed their differential expression between hypoxic exosomes and normoxic exosomes from ucMSCs by quantitative PCR. The expression of miR-125b was found to be most notably increased in hypoxic exosomes compared with normoxic exosomes (Figure 3A). To explore the correlation of the miR-125b levels in exosomes and their source ucMSCs, we assessed the expression of miR-125b in ucMSCs exposed to hypoxic conditions, including a tri-gas culture for 3 h and 6 h or stimulation with cobalt chloride ($CoCl_2$) to create a chemical hypoxia model. We observed an upregulation of miR-125b expression in ucMSCs cultured under hypoxic conditions (Figures 3B and 3C). A luciferase assay also confirmed increased reporter activity of the miR-125b promoter under hypoxic conditions (Figure 3D). These data suggested that the accumulation of miR-125b in exosomes was largely due to its upregulation in ucMSCs under hypoxic conditions.

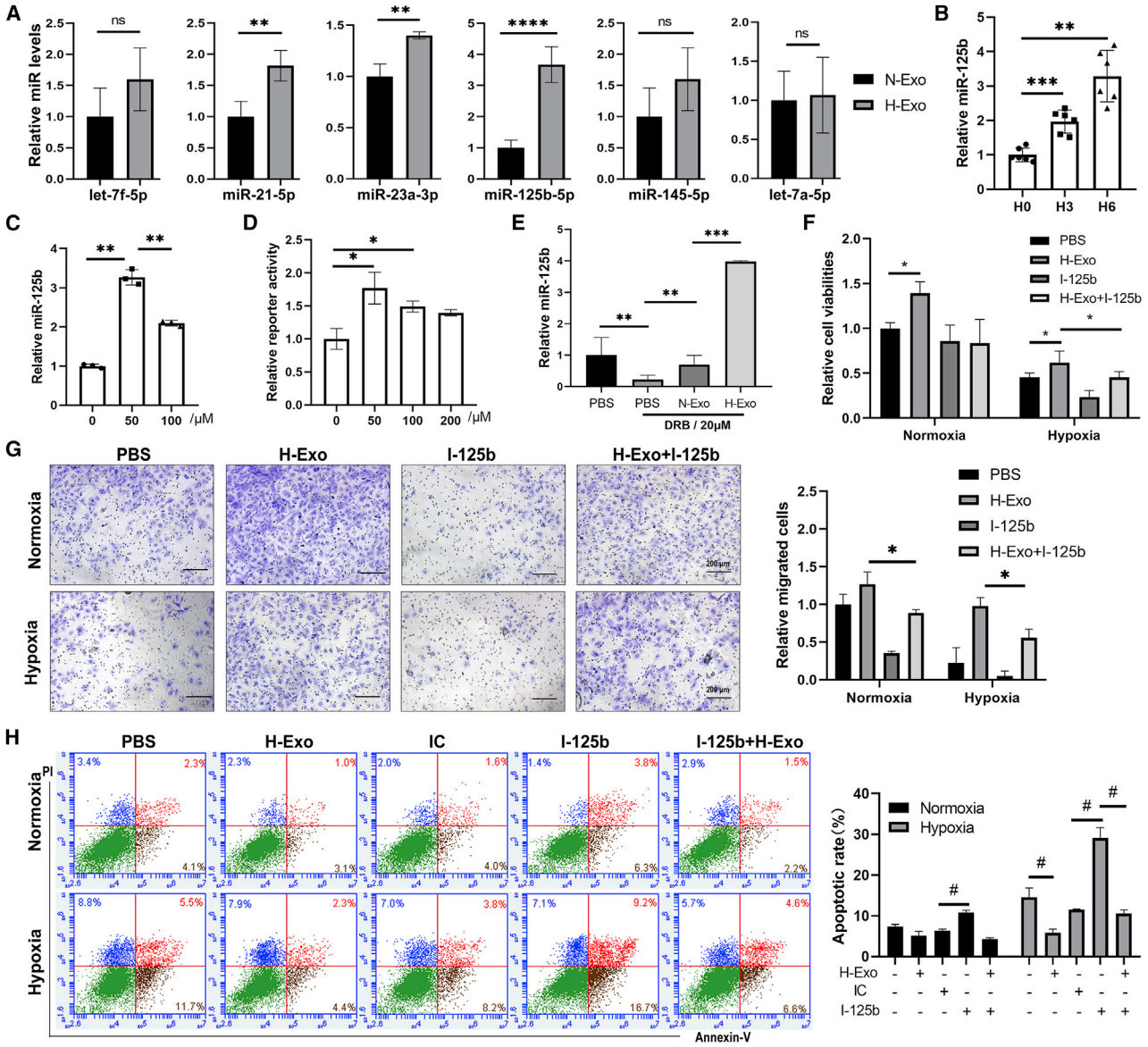

Figure 3. Hypoxic exosomal miR-125b promotes cell proliferation, migration, and survival of endothelial cells under hypoxic conditions

(A) The RNA levels of let-7f-5p, miR-21-5p, miR-23a-3p, miR-125b-5p, miR-145-5p, and let-7a-5p in H-Exos or N-Exos from ucMSCs. $^{**}p < 0.01$, $^{****}p < 0.0001$. ns, no significance. (B and C) miR-125b levels in ucMSCs placed into three gas incubators and exposed to hypoxia for 1 h and 3 h (B) or 50 μM $CoCl_2$ treatment for 8 h (C). $^{**}p < 0.01$, $^{***}p < 0.001$. (D) Luciferase assay to analyze the promoter activity of miR-125b in ucMSCs exposed to 50 μM $CoCl_2$ for 8 h. $^{*}p < 0.05$. (E) The expression of mature miR-125b in HUVECs treated with DRB (20 mM, 5,6-dichloro-1-β-D-ribofuranosylbenzimidazole, an RNA polymerase II inhibitor) for 48 h and H-Exos or N-Exos for another 48 h. $^{**}p < 0.01$, $^{***}p < 0.001$. (F) CCK-8 analysis of HUVEC proliferation following the indicated treatment. $^{*}p < 0.05$. (G) Representative images (left panel) and quantitative analysis (right panel) of Transwell migration assays of HUVECs after different treatments. Scale bar, 200 μm; $^{*}p < 0.05$. (H) Flow cytometry analysis of the apoptosis of HUVECs treated with the indicated exosomes or oligos (upper panel). Quantitative analysis of flow cytometry data (lower panel). #$p < 0.05$. The data are presented as the mean ± SD.

To further confirm whether exosomal miR-125b could be taken up by endothelial cells, we cocultured normoxic exosomes or hypoxic exosomes with HUVECs for 48 h, and the HUVECs were pretreated with 5,6-dichloro-1-β-D-ribofuranosylbenzimidazole (DRB, an RNA polymerase II inhibitor, 20 mM) for the previous 48 h. Then, we detected the expression of mature miR-125b in the HUVECs. DRB treatment markedly decreased the endogenous expression of mature miR-125b in HUVECs; exosome addition obviously improved the level of mature miR-125b, indicating that the increase in miR-125b expression in HUVECs was due to their uptake from exosomes rather than the enhanced transcription of miR-125b in HUVECs. Consistent with the dramatic

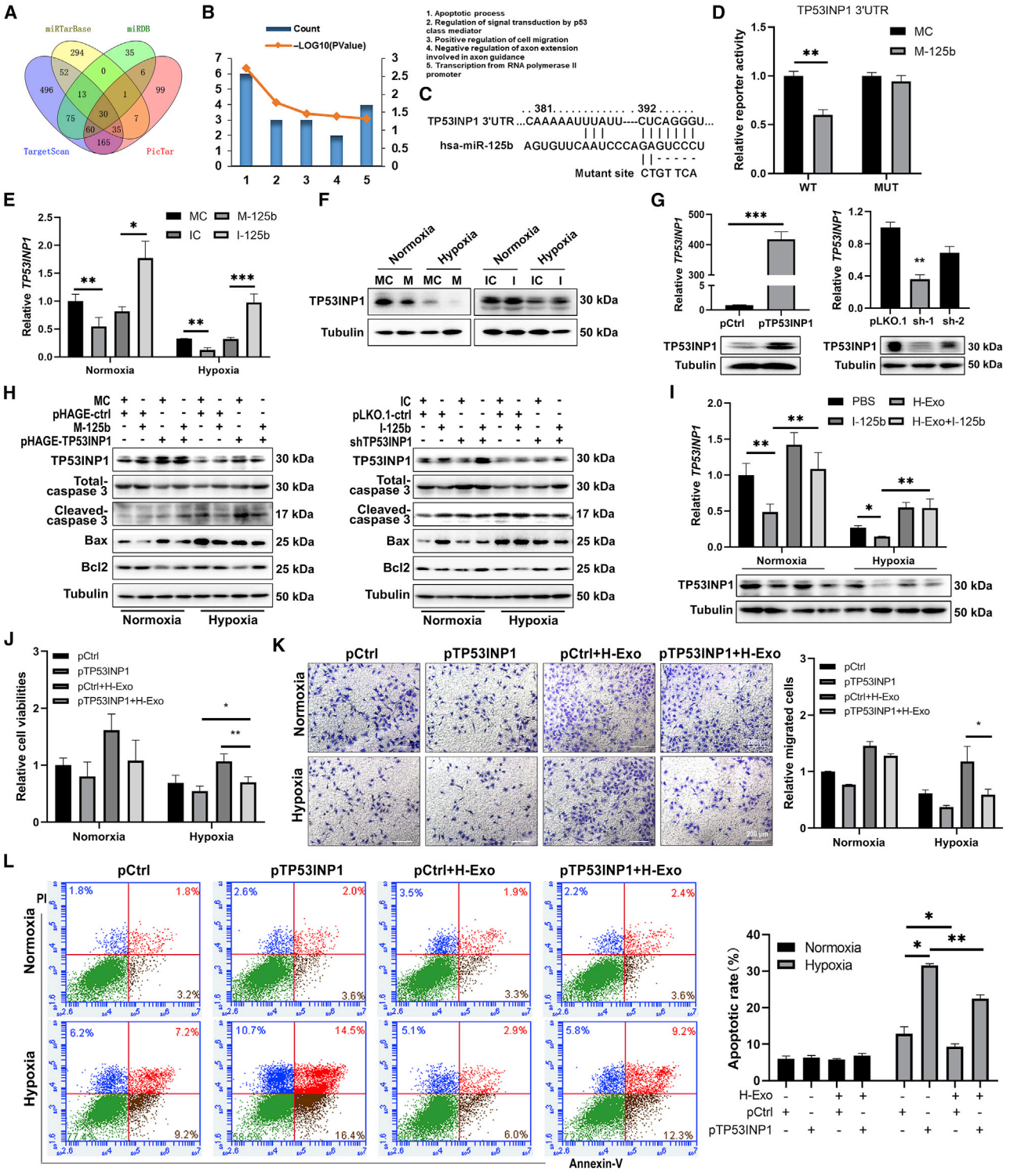

Figure 4. Exosomal miR-125b targets TP53INP1 in endothelial cells

(A) The predicted targets of miR-125b in four databases. (B) DAVID analysis of 30 common targets of miR-125b. (C) The binding site between hsa-miR-125b and TP53INP1. (D) The reporter activity of the 3′ untranslated region of *TP53INP1* in HUVECs transfected with miR-125b mimics or control oligos. **p < 0.01. (E and F) The mRNA and protein

(legend continued on next page)

increase in miR-125b expression in hypoxic exosomes, as shown in Figure 3A, the level of mature miR-125b expression in hypoxic exosome-treated HUVECs was much higher than that in normoxic exosome-treated HUVECs. The above data, together with the cytoplasmic localization of exosomes in endothelial cells (Figure 2C), further demonstrated much more uptake by HUVECs of miR-125b from hypoxic exosomes than of miR-125b from normoxic exosomes (Figure 3E).

To further address whether the function of exosomes depends on miR-125b, we treated HUVECs with hypoxic exosomes with or without miR-125b inhibitors. As CCK-8 (Figure 3F) and migration assays (Figure 3G) showed, inhibition of miR-125b blocked the promoting effect of hypoxic exosomes on cell growth and migration. Consistent with the *in vivo* study results (Figures 2F and 2G), hypoxic exosome treatment significantly decreased the cell apoptosis induced by high concentrations of $CoCl_2$, while inhibition of miR-125b abrogated the protective effect of hypoxic exosomes on cell apoptosis (Figure 3H). Taken together, we demonstrated that ucMSC-derived exosomal miR-125b, whose transcription was induced by hypoxic conditions, was necessary for cell migration and survival of endothelial cells.

The interaction of miR-125b and TP53INP1 is crucial for the function of hypoxic exosomes

MicroRNAs participate in diverse cellular signaling pathways by regulating their targets. To examine the functional mechanism of exosomal miR-125b in endothelial cells, we analyzed the targets of miR-125b using online databases, including TargetScan (http://www.targetscan.org/vert_72/), miRTarBase (https://mirtarbase.cuhk.edu.cn/~miRTarBase/miRTarBase_2019/php/download.php), miRDB (http://mirdb.org/), and PicTar (https://pictar.mdc-berlin.de/), and screened 30 common targets (Figure 4A). DAVID analysis showed that these targets were enriched in the cell apoptotic process ($p = 0.0018$), and tumor protein p53 inducible nuclear protein 1 (*TP53INP1*) was an interesting target mRNA of them (Figures 4B and 4C). Luciferase reporter assay confirmed the direct binding of miR-125b to the 3′ untranslated region of wild-type *TP53INP1* (Figure 4D). Then the expression of TP53INP1 was detected by quantitative PCR and western blotting. The mRNA and protein levels of TP53INP1 were obviously downregulated in endothelial cells by exposure to hypoxia (Figures 4E and 4F), indicating the involvement of TP53INP1 in hypoxia-induced cell damage. miR-125b overexpression suppressed the level of TP53INP1 under both normoxic and hypoxic conditions, and vice versa, suggesting that miR-125b increased the mRNA degradation of TP53INP1 (Figures 4E and 4F).

To further study the interaction of miR-125b and TP53INP1, we constructed stable *TP53INP1*-overexpressing or *TP53INP1*-knockdown HUVECs using a lentivirus delivery system (Figure 4G). Then, we verified the role of the interaction of miR-125b and TP53INP1 in the process of endothelial cell apoptosis by determining the protein levels of TP53INP1 and cell apoptotic markers, including caspase-3, B cell lymphoma 2-associated X protein (Bax), and B cell lymphoma 2 (Bcl2). As Figure 4H demonstrates, overexpression of miR-125b decreased the levels of cleaved caspase-3 and Bax and increased the level of Bcl2 in HUVECs treated with high concentrations of $CoCl_2$. Cotransfection of *TP53INP1* without the 3′ untranslated region reversed the effect of miR-125b overexpression on the above protein levels. Moreover, inhibition of miR-125b upregulated cleaved caspase 3, and Bax expression and downregulated Bcl2 expression, whereas cotransfection of *shTP53INP1* impaired the promotion effect of miR-125b inhibitors on cell apoptosis, indicating that the function of miR-125b during hypoxia was due, at least in part, to the downregulation of TP53INP1 expression (Figure 4H).

To identify whether the protective effect of hypoxic exosomes on endothelial cells was dependent on TP53INP1 downregulation, we analyzed the mRNA and protein levels of TP53INP1 following exosome treatment. Hypoxic exosome treatment reduced the level of TP53INP1, while inhibition of miR-125b abrogated this suppressive effect under hypoxic conditions (Figure 4I). Then, cell growth, migration, and survival were assessed under both normoxic and hypoxic conditions. As CCK-8 assays showed (Figure 4J), TP53INP1 overexpression led to lower cell viability than the corresponding control. Hypoxic exosome treatment improved cell viability, whereas the protective effect was reversed by TP53INP1 overexpression (Figure 4J). A similar phenomenon was observed in the migration assay; hypoxic exosomes increased the number of migrated cells, whereas TP53INP1 overexpression inhibited the promoting effect of hypoxic exosomes following hypoxia stimulation (Figure 4K). Apoptosis of *TP53INP1*-overexpressing endothelial cells exposed to hypoxia was also detected. As expected, we observed a higher cell apoptotic rate in hypoxic exosome-treated *TP53INP1*-overexpressing cells than in hypoxic exosome-treated control cells (Figure 4L). The data described above further illustrated that exosomal miR-125b targeted *TP53INP1* mRNA in endothelial cells and that the interaction of miR-125b and TP53INP1 was crucial for the function of exosomes.

Artificial miR-125b promotes cutaneous wound healing

To further determine the function of miR-125b in skin wound repair *in vivo*, we injected agomiR-125b or agomiR control oligos into the areas adjacent to skin injury sites by subcutaneous injection.

levels of TP53INP1 in HUVECs transfected with the indicated oligos under normoxic or hypoxic (200 μM $CoCl_2$ for 48 h) conditions. *$p < 0.05$, **$p < 0.01$, ***$p < 0.001$. (G) The mRNA and protein levels of TP53INP1 in HUVECs stably transfected with the indicated plasmids. **$p < 0.01$, ***$p < 0.001$. (H) Western blot analysis of the protein levels of TP53INP1, total caspase 3, cleaved caspase-3, Bax, and Bcl2 in HUVECs stably transfected with the indicated plasmids. (I) The mRNA and protein levels of TP53INP1 in HUVECs transfected with the indicated exosomes or oligos under normoxic or hypoxic (100 μM $CoCl_2$ for 48 h) conditions. *$p < 0.05$, **$p < 0.01$. (J) CCK-8 analysis of HUVEC proliferation following the indicated treatments. *$p < 0.05$, **$p < 0.01$. (K) Representative images (left panel) and quantitative analysis (right panel) of Transwell migration assays of HUVECs after different treatments. Scale bar, 200 μm; *$p < 0.05$. (L) Flow cytometry analysis of the apoptosis of HUVECs after different treatments (upper panel). Quantitative analysis of flow cytometry data (lower panel). *$p < 0.05$, **$p < 0.01$. The data are presented as the mean ± SD.

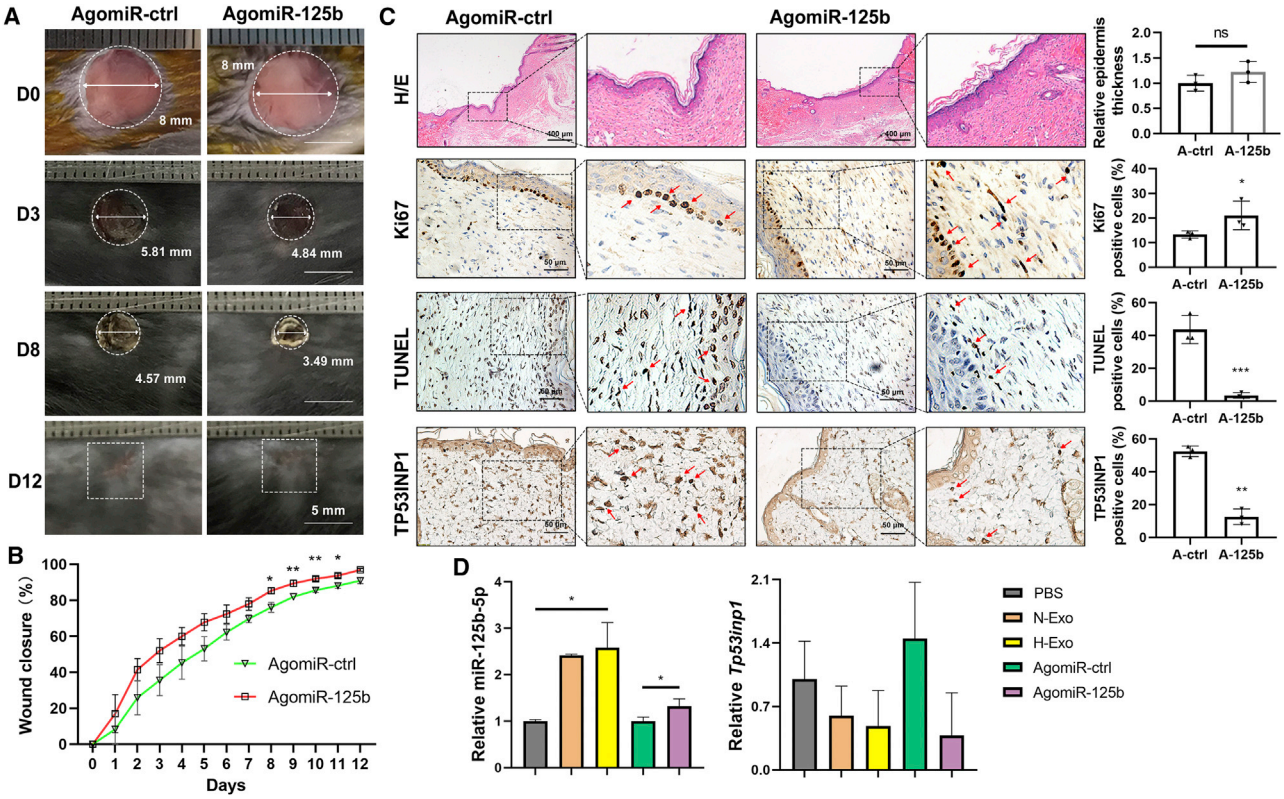

Figure 5. AgomiR-125b enhances cutaneous wound healing

(A) Gross view of wound areas of mice injected with agomiR control or agomiR-125b. Scale bar, 5 mm. Line segments with arrows represent the diameters of wound areas. The wound areas at D0, D3, and D8 are outlined with a circular dotted box, and with a square dotted box at D12 due to the difficulty in defining the border. (B) Quantification of wound-closure rates. *p < 0.05, **p < 0.01 versus agomiR control group. n = 5. (C) Representative images of H&E staining, Ki67 staining, TUNEL staining, and TP53INP1 staining of wound sections at day 12 post wounding (left panel). The right panel shows, from top to bottom, the thickness of the newly formed epidermis, the number of Ki67-positive cells, the number of TUNEL-positive cells, and the number of TP53INP1-positive cells. Scale bar, 400 μm in H&E staining and 50 μm in Ki67 and TUNEL staining. ns, no significance, *p < 0.05, **p < 0.01, ***p < 0.001. (D) The RNA levels of miR-125b and *Tp53inp1* in wound areas of mice injected with the indicated exosomes or oligos at day 12 post wounding. *p < 0.05. The data are presented as the mean ± SD.

Compared with the agomiR control group, agomirR-125b led to an apparent decrease in wounds at day 3 and the following days (Figure 5A). The wound closure rate of the agomiR-125b group was higher than that of the agomiR control group, as shown in Figure 5B. AgomiR-125b injection led to a slight increase in the thickness of the newly formed epidermis of 49.8 ± 12.3 μm compared with that of the agomiR control group of 40.7 ± 9.9 μm, but the difference was not statistically significant (Figure 5C). The number of Ki67-positive cells increased and the number of TUNEL-positive cells decreased following agomiR-125b treatment (Figure 5C). The expression of TP53INP1 was also tested, and we observed a reduction in TP53INP1 levels in the agomiR-125b group (Figure 5C). Then, the RNA levels of miR-125b and *Tp53inp1* in the wound sites of exosome- or oligo-treated animals at the end point of injury repair were detected by quantitative PCR, and the results showed that the expression of miR-125b was increased following exosome injection (Figure 5D, left). Although there was no significant difference in the mRNA levels of *Tp53inp1* among the five groups, *Tp53inp1* expression was lower in the exosome- or agomiR-125b-injected groups (Figure 5D, right). All these data further defined the interaction of miR-125b and TP53INP1 during exosome-mediated skin tissue repair.

DISCUSSION

Numerous studies have revealed the beneficial effect of MSCs in the repair of various tissues or organs; however, clinical trials of the utilization of MSCs in patients remain cautious due to the low survival and possible inflammatory responses elicited by MSCs.[32–34] Exosomes secreted by MSCs play a significant role in both intercellular communications and interactions with cellular microenvironments. Evidence has also accumulated that exosomes can be used as effective nanocarriers in cell-free-based tissue regeneration; they could modulate inflammation and promote proliferation and angiogenesis, similar to their source cells.[35–38] Nevertheless, although the current results of exosomes are encouraging, additional research is necessary to optimize the cell source of exosomes, to optimize the culture

condition of MSCs, and to understand the mechanism by which exosomes function in various microenvironments.

In the present study, ucMSCs were chosen due to their similar gene expression to that of skin fibroblasts and their pro-keratinocyte differentiation potential.[5,6] Both normoxic and hypoxic exosomes derived from ucMSCs increased the behaviors of endothelial cells and facilitated wound healing, suggesting that ucMSCs could serve as a good cell source for exosomes in skin regeneration. We have reported that ucMSCs could communicate with endothelial cells and enhance the function of gelatin methacryloyl hydrogel-based engineered skin.[22] Here, we found that the protective paracrine effect of ucMSCs on endothelial cells was mainly mediated by exosomes, as indicated by the loss of function of ucMSCs after GW4869 pretreatment. *In vivo* experiments also demonstrated that exosomes derived from ucMSCs indeed facilitated wound healing, which is consistent with previous reports.[18,19]

Several reports have demonstrated that hypoxic exosomes enhance cell proliferation and angiogenesis during myocardial infarction or tumor development.[31,40,41] In the present study, we found that hypoxic exosomes enhanced endothelial cell proliferation and migration *in vitro*, improving the quality of regenerated skin and conferring a higher proliferation rate and lower apoptosis rate, although their effect on the wound closure rate was comparable to that of normoxic exosomes. However, there are several limitations to the study. First, our present study only focused on the communication of exosomes with endothelial cells. In fact, Ki67 or TUNEL staining differences in other skin cell types, including basal cells and fibroblasts, were present in the PBS-treated group and exosome-treated groups, suggesting a direct or indirect interaction of these cells with exosomes, which should be addressed in our further study. In addition, we observed that there was no statistical difference in the epidermal thicknesses among normoxic exosome-, hypoxic exosome-, or PBS-treated groups, which suggested that the impact of exosomes on epidermal remodeling is not prominent. Indeed, the thickness of the newly formed epidermis is the comprehensive effect of exosomes on the specific epidermal cells and proteins, especially keratinocytes and keratins, which were arranged in an orderly fashion to form the structure of epidermis. Our study is limited to the protective effect of exosomes on endothelial cells. In future studies, the impact of exosomes on the organization of keratinocytes and keratins should be further clarified. In addition, it is possible that day 12 is not an optimal time to observe the thickness of regenerated epidermis in our study. Second, we only evaluated the effect of the two types of exosomes at day 12, after healing was almost complete, and their effects on the phases of inflammation and reepithelialization occurring at the early stages of wound repair require further study. It is noteworthy that wound healing in a mouse is fundamentally different from that of humans, as it primarily occurs via contraction.[42] A splint incorporated around the wounds of mice or a rat full-thickness skin injury model could better simulate the conditions of human skin repair.[42]

Physical (tri-gas incubator) and chemical ($CoCl_2$) hypoxia models were used in our study. The duration of stimulation or concentration of chemicals should be addressed. Although the mechanisms of the two hypoxic conditions were different, we observed a significant induction of miR-125b expression under both conditions. The tri-gas incubator sustainably increased miR-125b expression over time, while a low concentration of $CoCl_2$ (50 μM) induced higher expression of miR-125b than a high concentration of $CoCl_2$ (100 μM). The effect of hypoxic exosomes under different hypoxic conditions was not explored in our present study. $CoCl_2$ might be more suited for large-scale cell culture to produce more exosomes due to its advantages of low cost, ease of use, and better control of the variable degrees of hypoxia. Collectively, further research is needed to optimize the hypoxic conditions and compare the functions of hypoxic exosomes under different hypoxic conditions.

Multiple studies have shown that exosomes communicate with target cells by delivering certain microRNAs. An elegant study previously analyzed the microRNA expression profiles of exosomes derived from ucMSCs or human embryonic kidney 293T cells, characterizing miR-21, miR-125b-5p, miR-23a-3p, miR-100-5p, let-7f-5p, let-7a-5p, and miR-145-5p as the first seven microRNAs with high abundances of 12.5%, 10.2%, 4.9%, 3.4%, 3.2%, 2.5%, and 2%, respectively.[18] We speculated that the abundance of microRNAs in exosomes was important for their functions, and therefore we chose the most highly abundant microRNAs and analyzed their levels in exosomes from ucMSCs cultured under normoxic and hypoxic conditions. We found a marked increase in the miR-125b levels in hypoxic exosomes from ucMSCs. miR-125b has also been reported to be increased in bone-marrow derived mesenchymal stem cell-derived exosomes after exposure to hypoxia,[31] which suggests that hypoxia-induced levels of miR-125b in exosomes might be a common phenomenon in MSCs.

The levels of microRNAs in exosomes were intensively correlated with their expression in their cells of origin.[27,28] We compared the expression of miR-125b in ucMSCs and 293T cells and observed that the miR-125b level was at least 10 times greater in ucMSCs than that in 293T cells in a quiescent state; exposure to hypoxia further induced miR-125b expression in both ucMSCs and 293T cells (data not shown). These results support the above conclusion, but the primary factors regulating the sorting of miR-125b or other microRNAs to exosomes following hypoxia stimulus require further study. It is also necessary to characterize the function of exosomes from different cell sources under various physiological conditions, as well as the underlying mechanisms, to provide a basis for their clinical application.

TP53INP1 is a protein with multiple functions and is involved in cell cycle arrest and apoptosis. In the present study, we showed that hypoxia profoundly suppressed TP53INP1 expression, suggesting the involvement of TP53INP1 in hypoxia-induced cell death. TP53INP1 is a known target of miR-125b in various diseases or cell processes, such as ischemia-reperfusion-induced neuroinflammation and endometrial cancer cell migration.[43,44] However, whether this interaction exists between exosomal miR-125b and TP53INP1 in targeted cells remains to be determined. We verified that the induction of cell

proliferation and migration and the inhibition of cell apoptosis by exosomal miR-125b were dependent on its interaction with TP53INP1, further indicating that TP53INP1 was an important target of miR-125b. The RNA level of miR-125b was increased at exosome- or agomiR-125b-injected wound sites in mice, whereas *Tp53inp1* expression was reduced in these groups, further indicating an interaction of miR-125b and TP53INP1. Overall, the miR-125b-TP53INP1 interaction was crucial for the function of endothelial cells.

Notably, we observed that inhibition of miR-125b expression did not entirely eliminate the protective effect of hypoxic exosomes in *in vitro* experiments. Our *in vivo* study also showed that the level of miR-125b in wound sites injected with exosomes was considerably higher than in those injected with agomiR-125b at day 12, which might be caused by factors such as (1) the inequality of miR-125b contents in exosomes (100 ng) and agomiR-125b (2 nM); (2) other protective components of exosomes, such as miR-21 and miR-23a;[18] or (3) better stability of exosomes *in vivo*. The results suggested a better effect of exosomes than agomiR oligos. In our further research, exosomes or oligos encapsulated in hydrogels will be used in a cutaneous repair model to compare their different therapeutic effects.

In conclusion, we demonstrated that hypoxic exosomes from ucMSCs enhanced skin wound repair by promoting cell growth and migration and decreasing cell apoptosis. Mechanistically, miR-125b, whose transcription was induced by hypoxia, was sorted into exosomes in ucMSCs. After internalization by endothelial cells, miR-125b targeted the 3′ untranslated region of *TP53INP1* mRNA and suppressed TP53INP1-mediated cell apoptosis, which finally led to cell survival and subsequent wound healing.

MATERIALS AND METHODS

Animals

All experimental procedures involving animals were approved by the Animal Care and Use Committee of Wuhan Union Hospital. All mice were housed in an environment with controlled light (12 h light/12 h dark), temperature (23°C ± 2°C), and humidity. 8-week-old male BALB/C mice were used. For the full-thickness skin wound model, mice were anesthetized by intraperitoneal (i.p.) administration of 50 mg/kg pentobarbital sodium. A skin wound 8 mm in diameter was created on the dorsum. In total, 25 mice were randomly divided into control group (PBS), normoxic or hypoxic exosome groups (200 μg in 100 μL PBS), and agomiR-125b or agomiR-control groups, with 5 mice in each group. The above exosomes or oligos were subcutaneously injected at four points around the wound sites. The wounds were photographed every day and the wound size was analyzed by ImageJ software. 12 days after injection, mice were sacrificed, and skin samples were harvested for further analysis. The wound-healing rate on a specific day (day X) was the ratio of the wound area differences between day 0 and day X to wound area at day 0.

Histology staining and TUNEL staining

Skin samples were fixed in 4% paraformaldehyde, dehydrated, embedded in paraffin, sectioned into 5-μm-thick pieces, and stained with H&E. For each mouse, epidermal thickness of regenerated skin flanked by the normal skin with hair follicles was measured from stratum basal to stratum corneum at six equidistant sites. Immunofluorescence staining for Ki67 (Servicebio, #GB111141, Wuhan, China) and TP53INP1 (ABclonal, #A8274) were performed to evaluate cell proliferation and the level of TP53INP1, respectively. TUNEL (terminal deoxynucleotidyl transferase dUTP nick end labeling) assays were performed to detect cell apoptosis according to the manufacturer's instructions (Servicebio, #G1507, Wuhan, China).

Exosome isolation and identification

ucMSCs (Cyagen, Guangdong, China) were cultured to a density of 2×10^7 cells/75 mm flask. Culture media were removed, and cells were washed three times with PBS and then cultured in serum-free media for 48 h. The media were collected, and cell debris was discarded by gradient centrifugation at 300 × *g* for 10 min and 10,000 × *g* for 30 min at 4°C. Further centrifugation (100,000 × *g*, 4°C, 70 min) was performed to obtain exosomes. The size distribution and zeta potential of exosomes was measured by Zetasizer Nano ZS90 (Malvern Panalytical, Westborough, MA, USA). The morphologies of exosomes were photographed with transmission electron microscopy (Hitachi HT 7800, Tokyo, Japan). The exosomes were measured for their protein content using the BCA protein assay kit (Pierce Protein Biology, Thermo Fisher Scientific Life Sciences). For labeling, exosomes were incubated with DIOC18(3), a green fluorescent lipophilic tracer (Beyotime), at room temperature for 30 min and centrifuged at 100,000 × *g*, 4°C, for 70 min, incubated with HUVECs in normoxic and hypoxic conditions for 3 h, and then photographed.

In vivo exosome tracking assay

To assess exosome uptake by skin endothelial cells, 20 μL DIOC18(3)-labeled exosomes (1 μg/μL) were injected into the around areas of wounded skin. Mice were sacrificed at 5 h after injection. The skin was dehydrated and frozen, then sliced into 10-μm-thick cryosections. The sections were incubated with primary antibody against von Willebrand factor (Servicebio, #GB11020, Wuhan, China) overnight at 4°C and then dyed with DAPI. The internalization of exosomes into skin endothelial cells was observed by confocal microscope.

Cell culture

ucMSCs and HUVECs were cultured in specific complete media (Cyagen, Guangdong, China). 293T were cultured in DMEM (Gibco) supplemented with 10% fetal bovine serum (FBS) and 100 U/mL penicillin-streptomycin (Gibco). For hypoxic treatment, cells were exposed to 1% O_2, 95% N_2, and 5% CO_2 for 3–6 h in a tri-gas incubator. When required, cells were treated with a high concentration of $CoCl_2$ (200 μM) for 24 h to induce cell growth arrest and apoptosis, while low concentration of $CoCl_2$ with 50 μM was used to induce the production of exosomes The optimal concentration of $CoCl_2$ (50 μM) was determined by dose-dependent (using 25–200 μM) experiments to produce maximal induction of HIF1α and miR-125b at 12 h, without affecting cell viabilities (data not shown). For coculture of

exosomes and cells, 50 μg/mL of exosomes were incubated with HUVECs at 37°C for 24 h.

Cell viability assay

CCK-8 assays were performed to analyze cellular proliferation and activity. HUVECs were seeded at a density of 2×10^3 cells/well in 96-well plates. At 24, 48, 72, 96, and 120 h, 10 μL of CCK-8 solution (Dojindo Laboratories, Kumamoto, Japan) was added to each well of the plate and incubated for 1 h. Cell viability was then determined using a spectrophotometer set (ELx800, BioTek, Winooski, VT, USA) at a wavelength of 450 nm.

Wound-healing assay

HUVEC migrations were performed in 12-well plates by wound-healing assays *in vitro*. Cells were seeded at a density of 5×10^5 cells per well and starved for 24 h. Wounds were made by scratching with a 200 μL pipette tip (3 wounds per well). The cell debris was removed with PBS washing. Then cells were incubated with supernatants from ucMSCs treated with or without hypoxic treatment. The scratch of each group was observed using a microscope at 0 h and 24 h. The area of the scratch was measured using ImageJ software.

Transwell migration assay

For Transwell assay, 3×10^4 cells were suspended in serum-free medium and seeded into the upper chamber of Transwell 24-well plates (8 μm pore filters, Corning, Corning, NY, USA). Complete medium with or without exosomes was added to the lower chamber. After 16 h, the cells on the upper surface of the inserts were wiped. Migrated cells of the lower surface were stained with crystal violet and photographed with a microscope.

Flow cytometry analysis

Cells treated with indicated exosomes or oligos were exposed to 200 μM $CoCl_2$ for 24 h, and cell apoptosis was tested using PI/Annexin V-FITC staining (#556547, BD Biosciences, St. Louis, MO, USA) according to the manufacturer's protocol for another 10 min. After incubation, the cells were subjected to apoptosis analysis using BD Accuri C6 Plus cytometer (Beckman Coulter, Fullerton, CA, USA), and the results were analyzed with BD Accuri C6 Plus software.

Plasmid and stable transfected cell lines

The mimics, inhibitors, and corresponding negative control oligos for hsa-miR-125b-5p were purchased from Guangzhou RiboBio (Guangzhou, China). Oligo transfection was performed as per manufacturer's instructions. Human *TP53INP1* cDNA was amplified following the primers: 5′-ATGGACAATATGTCTATTAC-3′ (forward) and 5′-TCAGTCTAAAGGTTGTGGG-3′ (reverse). The short hairpin RNA (shRNA) sequences against *TP53INP1* were as follows: (1) 5′-CGAGTTGTATCACCTGGAATT-3′, (2) 5′-GTACTTCATA CCATGCCGATT-3′, and (3) the scramble sequence, 5′-AATT CTCCGAACGTGTCACGT-3′. The cDNAs were ligated into pHAGE-flag vector, and shRNAs were ligated into pLKO.1 vector. For stable cell line construction, HEK293T cells were transfected with overexpression or knockdown plasmids with packaging plasmids pSPAX2 and pMD2G for 60 h. The supernatants were harvested, filtered with 0.22 μm membrane, and added into pre-seeded HUVECs in a 6-well plate. Puromycin (2 μg/mL) was utilized to screen stable expression clones.

Luciferase reporter assay

293T cells were seeded in 24-well plates at a density of 2×10^5 cells/well and transfected with the indicated plasmids for 24 h. Luciferase assays were performed using a dual-luciferase assay kit (#E1960, Promega, Madison, WI, USA) according to the manufacturer's instructions.

Quantitative PCR

Total RNA was extracted using TRIzol reagent (#9109, TaKaRa, Japan). cDNA was obtained by using an oligo (dT) primer and reverse transcriptase (Thermo Fisher Scientific, Waltham, MA, USA) following standard protocols. MicroRNA was reverse transcribed by using specific Bulge-Loop RT primers (RiboBio, Guangzhou, China). The relative expression levels of mRNA and microRNA were normalized to GAPDH or U6, respectively.

Western blot

Cells were lysed in RIPA lysis buffer (#P00138, Beyotime Biotechnology, Shanghai, China). Equal amounts of protein were separated by SDS-PAGE gels and transferred to polyvinylidene fluoride (PVDF) membrane. Antibodies against CD9 (#A19027), CD63 (#A5271), CD81 (#A5270), and HSP70 (#A0284) were obtained from ABclonal Technology (ABclonal, Wuhan, China). The antibodies against HIF1α (#36169, Cell Signaling Technology [CST], Danvers, MA, USA), Bax (#5023, CST, Danvers, MA, USA), Bcl-2 (#15071, CST, Danvers, MA, USA), caspase3 (#9665, CST, Danvers, MA, USA), cleved-caspase3 (#9661, CST, Danvers, MA, USA), p53 (#9282, CST, Danvers, MA, USA), and β-tubulin (#2128, CST, Danvers, MA, USA) were purchased from Cell Signaling Technology. A ChemiDoc MP Imaging System (Bio-Rad, Hercules, CA, USA) was used for signal detection.

Statistical analysis

All the data in this study are expressed as means ± SD. Two treatment groups were compared by Student's t test. Multiple groups were analyzed by one-way ANOVA analysis. GraphPad Prism version 8.0 was used for statistical analyses. Statistical significance was considered when $p < 0.05$.

ACKNOWLEDGMENTS

This study was supported by grants from the National Natural Science Foundation of China (no. 81801923, no. 81700558, no. 81570570, no. 81670575, and no. 81070355), the Program of HUST Academic Frontier Youth Team (2018QYTD02), and the Pre-Research Fund for Free Innovation of Union Hospital, Huazhong University of Science and Technology (no. 02.03.2017-312, no. 02.03.2017-59, and no. 02.03.2018-126). We would like to thank

Ying Liu and the Core Facility of Medical Research Institute at Wuhan University for flow cytometry and histological analysis.

AUTHOR CONTRIBUTIONS

X.-F.Z. and H.W. designed the topic and performed statistical analyses. X.-F.Z., T.W., Z.-X.W., and K.-P.H. performed animal experiments. X.-F.Z., Z.-X.W., and T.W. performed function studies. Z.-X.W., T.W., Y.-W.Z., G.-L.W., H.-J.Z., Z.-H.C., and C.-Y.W. performed mechanism studies. X.-F.Z., H.W., and J.-X.Z. wrote the manuscript. All authors discussed the results and reviewed and approved the final manuscript.

DECLARATION OF INTERESTS

The authors declare no competing interests.

REFERENCES

1. Nourian Dehkordi, A., Mirahmadi Babaheydari, F., Chehelgerdi, M., and Raeisi Dehkordi, S. (2019). Skin tissue engineering: wound healing based on stem-cell-based therapeutic strategies. Stem Cell Res. Ther. *10*, 111.
2. Petrof, G., Abdul-Wahab, A., and McGrath, J.A. (2014). Cell therapy in dermatology. Cold Spring Harb. Perspect. Med. *4*, a015156.
3. Sun, B.K., Siprashvili, Z., and Khavari, P.A. (2014). Advances in skin grafting and treatment of cutaneous wounds. Science *346*, 941–945.
4. Pereira, R.F., Barrias, C.C., Granja, P.L., and Bartolo, P.J. (2013). Advanced biofabrication strategies for skin regeneration and repair. Nanomedicine (Lond.) *8*, 603–621.
5. Schneider, R.K., Püllen, A., Kramann, R., Bornemann, J., Knüchel, R., Neuss, S., and Perez-Bouza, A. (2010). Long-term survival and characterisation of human umbilical cord-derived mesenchymal stem cells on dermal equivalents. Differentiation *79*, 182–193.
6. Chen, D., Hao, H., Tong, C., Liu, J., Dong, L., Ti, D., Hou, Q., Liu, H., Han, W., and Fu, X. (2015). Transdifferentiation of Umbilical Cord-Derived Mesenchymal Stem Cells Into Epidermal-Like Cells by the Mimicking Skin Microenvironment. Int. J. Low. Extrem. Wounds *14*, 136–145.
7. Kurtz, A. (2008). Mesenchymal stem cell delivery routes and fate. Int. J. Stem Cells *1*, 1–7.
8. Zhang, X., Sai, B., Wang, F., Wang, L., Wang, Y., Zheng, L., Li, G., Tang, J., and Xiang, J. (2019). Hypoxic BMSC-derived exosomal miRNAs promote metastasis of lung cancer cells via STAT3-induced EMT. Mol. Cancer *18*, 40.
9. Kim, H., Wang, S.Y., Kwak, G., Yang, Y., Kwon, I.C., and Kim, S.H. (2019). Exosome-Guided Phenotypic Switch of M1 to M2 Macrophages for Cutaneous Wound Healing. Adv. Sci. (Weinh.) *6*, 1900513.
10. Kalluri, R., and LeBleu, V.S. (2020). The biology, function, and biomedical applications of exosomes. Science *367*, eaau6977.
11. Pegtel, D.M., and Gould, S.J. (2019). Exosomes. Annu. Rev. Biochem. *88*, 487–514.
12. Zhai, M., Zhu, Y., Yang, M., and Mao, C. (2020). Human Mesenchymal Stem Cell Derived Exosomes Enhance Cell-Free Bone Regeneration by Altering Their miRNAs Profiles. Adv. Sci. (Weinh.) *7*, 2001334.
13. Fan, J., Lee, C.S., Kim, S., Chen, C., Aghaloo, T., and Lee, M. (2020). Generation of Small RNA-Modulated Exosome Mimetics for Bone Regeneration. ACS Nano *14*, 11973–11984.
14. Fuhrmann, G., Chandrawati, R., Parmar, P.A., Keane, T.J., Maynard, S.A., Bertazzo, S., and Stevens, M.M. (2018). Engineering Extracellular Vesicles with the Tools of Enzyme Prodrug Therapy. Adv. Mater. *30*, e1706616.
15. McLaughlin, M., Patin, E.C., Pedersen, M., Wilkins, A., Dillon, M.T., Melcher, A.A., and Harrington, K.J. (2020). Inflammatory microenvironment remodelling by tumour cells after radiotherapy. Nat. Rev. Cancer *20*, 203–217.
16. Xu, R., Rai, A., Chen, M., Suwakulsiri, W., Greening, D.W., and Simpson, R.J. (2018). Extracellular vesicles in cancer - implications for future improvements in cancer care. Nat. Rev. Clin. Oncol. *15*, 617–638.
17. Xue, M., Chen, W., Xiang, A., Wang, R., Chen, H., Pan, J., Pang, H., An, H., Wang, X., Hou, H., and Li, X. (2017). Hypoxic exosomes facilitate bladder tumor growth and development through transferring long non-coding RNA-UCA1. Mol. Cancer *16*, 143.
18. Fang, S., Xu, C., Zhang, Y., Xue, C., Yang, C., Bi, H., Qian, X., Wu, M., Ji, K., Zhao, Y., et al. (2016). Umbilical Cord-Derived Mesenchymal Stem Cell-Derived Exosomal MicroRNAs Suppress Myofibroblast Differentiation by Inhibiting the Transforming Growth Factor-β/SMAD2 Pathway During Wound Healing. Stem Cells Transl. Med. *5*, 1425–1439.
19. Hu, Y., Rao, S.S., Wang, Z.X., Cao, J., Tan, Y.J., Luo, J., Li, H.M., Zhang, W.S., Chen, C.Y., and Xie, H. (2018). Exosomes from human umbilical cord blood accelerate cutaneous wound healing through miR-21-3p-mediated promotion of angiogenesis and fibroblast function. Theranostics *8*, 169–184.
20. Niinikoski, J., Grislis, G., and Hunt, T.K. (1972). Respiratory gas tensions and collagen in infected wounds. Ann. Surg. *175*, 588–593.
21. Desmet, C.M., Préat, V., and Gallez, B. (2018). Nanomedicines and gene therapy for the delivery of growth factors to improve perfusion and oxygenation in wound healing. Adv. Drug Deliv. Rev. *129*, 262–284.
22. Zhang, X., Li, J., Ye, P., Gao, G., Hubbell, K., and Cui, X. (2017). Coculture of mesenchymal stem cells and endothelial cells enhances host tissue integration and epidermis maturation through AKT activation in gelatin methacryloyl hydrogel-based skin model. Acta Biomater *59*, 317–326.
23. Rani, S., Ryan, A.E., Griffin, M.D., and Ritter, T. (2015). Mesenchymal Stem Cell-derived Extracellular Vesicles: Toward Cell-free Therapeutic Applications. Mol. Ther. *23*, 812–823.
24. Wang, J., Xia, J., Huang, R., Hu, Y., Fan, J., Shu, Q., and Xu, J. (2020). Mesenchymal stem cell-derived extracellular vesicles alter disease outcomes via endorsement of macrophage polarization. Stem Cell Res. Ther. *11*, 424.
25. Phinney, D.G., and Pittenger, M.F. (2017). Concise Review: MSC-Derived Exosomes for Cell-Free Therapy. Stem Cells *35*, 851–858.
26. Kourembanas, S. (2015). Exosomes: vehicles of intercellular signaling, biomarkers, and vectors of cell therapy. Annu. Rev. Physiol. *77*, 13–27.
27. Temoche-Diaz, M.M., Shurtleff, M.J., Nottingham, R.M., Yao, J., Fadadu, R.P., Lambowitz, A.M., and Schekman, R. (2019). Distinct mechanisms of microRNA sorting into cancer cell-derived extracellular vesicle subtypes. eLife *8*, e47544.
28. Squadrito, M.L., Baer, C., Burdet, F., Maderna, C., Gilfillan, G.D., Lyle, R., Ibberson, M., and De Palma, M. (2014). Endogenous RNAs modulate microRNA sorting to exosomes and transfer to acceptor cells. Cell Rep. *8*, 1432–1446.
29. Kumar, A., and Deep, G. (2020). Hypoxia in tumor microenvironment regulates exosome biogenesis: Molecular mechanisms and translational opportunities. Cancer Lett. *479*, 23–30.
30. Li, Z.L., Lv, L.L., Tang, T.T., Wang, B., Feng, Y., Zhou, L.T., Cao, J.Y., Tang, R.N., Wu, M., Liu, H., et al. (2019). HIF-1α inducing exosomal microRNA-23a expression mediates the cross-talk between tubular epithelial cells and macrophages in tubulointerstitial inflammation. Kidney Int. *95*, 388–404.
31. Zhu, L.P., Tian, T., Wang, J.Y., He, J.N., Chen, T., Pan, M., Xu, L., Zhang, H.X., Qiu, X.T., Li, C.C., et al. (2018). Hypoxia-elicited mesenchymal stem cell-derived exosomes facilitates cardiac repair through miR-125b-mediated prevention of cell death in myocardial infarction. Theranostics *8*, 6163–6177.
32. Bunpetch, V., Zhang, Z.Y., Zhang, X., Han, S., Zongyou, P., Wu, H., and Hong-Wei, O. (2019). Strategies for MSC expansion and MSC-based microtissue for bone regeneration. Biomaterials *196*, 67–79.
33. Goradel, N.H., Hour, F.G., Negahdari, B., Malekshahi, Z.V., Hashemzehi, M., Masoudifar, A., and Mirzaei, H. (2018). Stem Cell Therapy: A New Therapeutic Option for Cardiovascular Diseases. J. Cell. Biochem. *119*, 95–104.
34. Mirzaei, H., Salehi, H., Oskuee, R.K., Mohammadpour, A., Mirzaei, H.R., Sharifi, M.R., Salarinia, R., Darani, H.Y., Mokhtari, M., Masoudifar, A., et al. (2018). The therapeutic potential of human adipose-derived mesenchymal stem cells producing CXCL10 in a mouse melanoma lung metastasis model. Cancer Lett. *419*, 30–39.

35. Zhang, D., Lee, H., Wang, X., Rai, A., Groot, M., and Jin, Y. (2018). Exosome-Mediated Small RNA Delivery: A Novel Therapeutic Approach for Inflammatory Lung Responses. Mol. Ther. *26*, 2119–2130.

36. Grange, C., Papadimitriou, E., Dimuccio, V., Pastorino, C., Molina, J., O'Kelly, R., Niedernhofer, L.J., Robbins, P.D., Camussi, G., and Bussolati, B. (2020). Urinary Extracellular Vesicles Carrying Klotho Improve the Recovery of Renal Function in an Acute Tubular Injury Model. Mol. Ther. *28*, 490–502.

37. Ghaemmaghami, A.B., Mahjoubin-Tehran, M., Movahedpour, A., Morshedi, K., Sheida, A., Taghavi, S.P., Mirzaei, H., and Hamblin, M.R. (2020). Role of exosomes in malignant glioma: microRNAs and proteins in pathogenesis and diagnosis. Cell Commun. Signal. *18*, 120.

38. Mianehsaz, E., Mirzaei, H.R., Mahjoubin-Tehran, M., Rezaee, A., Sahebnasagh, R., Pourhanifeh, M.H., Mirzaei, H., and Hamblin, M.R. (2019). Mesenchymal stem cell-derived exosomes: a new therapeutic approach to osteoarthritis? Stem Cell Res. Ther. *10*, 340.

40. Yue, X., Lan, F., and Xia, T. (2019). Hypoxic Glioma Cell-Secreted Exosomal miR-301a Activates Wnt/β-catenin Signaling and Promotes Radiation Resistance by Targeting TCEAL7. Mol. Ther. *27*, 1939–1949.

41. Hsu, Y.L., Hung, J.Y., Chang, W.A., Lin, Y.S., Pan, Y.C., Tsai, P.H., Wu, C.Y., and Kuo, P.L. (2017). Hypoxic lung cancer-secreted exosomal miR-23a increased angiogenesis and vascular permeability by targeting prolyl hydroxylase and tight junction protein ZO-1. Oncogene *36*, 4929–4942.

42. Wang, X., Ge, J., Tredget, E.E., and Wu, Y. (2013). The mouse excisional wound splinting model, including applications for stem cell transplantation. Nat. Protoc. *8*, 302–309.

43. Li, X.Q., Yu, Q., Tan, W.F., Zhang, Z.L., and Ma, H. (2018). MicroRNA-125b mimic inhibits ischemia reperfusion-induced neuroinflammation and aberrant p53 apoptotic signalling activation through targeting TP53INP1. Brain Behav. Immun. *74*, 154–165.

44. Jiang, F., Liu, T., He, Y., Yan, Q., Chen, X., Wang, H., and Wan, X. (2011). MiR-125b promotes proliferation and migration of type II endometrial carcinoma cells through targeting TP53INP1 tumor suppressor in vitro and in vivo. BMC Cancer *11*, 425.